

Temporal and Spatial Characteristics of Positive and Negative Indian Ocean Dipole with and without ENSO

Chi-Cherng Hong

Department of Science, TMUE/Taiwan,

Mong-Ming Lu

Central Weather Bureau, Taiwan

Masao Kanamitsu

Scripps Institution of Oceanography, UCSD

Abstract

The differences in the temporal evolution and spatial characteristics of the Indian Ocean Dipole (IOD) between positive and negative events with and without ENSO have been investigated using observations for the period 1948-2002. To document such differences is particularly important for climate forecasts over Far East Asia, since distinctly different monsoon activities over China, Korea and Japan for different types of IOD are found in the composite maps of precipitation anomalies. The composite map of SST and wind during various stages of IOD and the ocean mixed layer heat budget showed that the IOD with and without ENSO has a large difference in its temporal evolutions and their triggering mechanisms. In both negative and positive IOD events without ENSO, the wind anomaly in the eastern Indian Ocean seems to be responsible for the formation of sea surface temperature anomalies, while the anomaly in the western Indian Ocean seems to be the oceanic dynamical response to the anomaly in the east. During the ENSO years, the temporal and spatial contrast of the asymmetry of the IOD evolution is smaller, and the SST anomaly is driven by the anomalies in incoming radiation due to changes in cloudiness caused by the ENSO associated anomalous atmospheric circulations and not by the local wind anomalies.

1. Introduction

The Indian Ocean Dipole (IOD) is one of the dominant modes of the inter-annual variability of the Indian Ocean SST (Saji et al. 1999; Webster et al. 1999). It has been argued that the IOD is an artificial mode (Dommenges and Latif 2002), or that it is an ENSO forced mode (Baquero-Bernal et al. 2002; Yu and Lau 2004). But recent studies show IOD is a physical mode and can be identified without ENSO (e.g., Ashok et al. 2004; Lau and Nath 2004; Behera et al. 2006).

In many of the published papers, we found that positive and negative phases of IODs are not treated

separately. We also noticed that the well documented (e.g., Vinayachandran et al. 1999; Yu and Rienecker 1999) strong IOD cases were all based on positive events, from which some of the studies of its mechanisms are based (Li et al. 2003; Zhong et al. 2005). The study of negative events was less common than the positive events and the difference in the temporal evolution of positive and negative IODs has not been documented well.

The influence of ENSO on IOD is another point of interest. It has been noted that ENSO remote forcing leads to an Indian Ocean basin scale warming in the

following spring after the ENSO matures (Xie et al. 2002). Nearly 40% of IODs occur simultaneously with ENSO; the positive IOD is associated with El Niño and the negative IOD generally with La Niña (Saji and Yamagata 2003; Ashok et al 2004). The warm and cold ENSO events do not evolve in the same way (with opposite sign) (An and Jin 2004). It was also recently demonstrated that the ENSO-Indian ocean coupling is different for warm and cold events (Kug et al. 2006).

From these views of the positive and negative phase of the IOD and its response to ENSO, we feel it is essential to re-examine the evolution of spatial structure of IOD for positive and negative phases as well as with and without ENSO, individually. The main purposes of this study are (1) to examine the relation between various IODs and the precipitation over Asia, (2) to describe the characteristics of time evolution and structure of the four types of IODs, (3) to examine the impact of ENSO on the IOD and (4) to interpret the physical mechanisms of the evolution of each IOD event.

2.Data

The monthly NCEP reanalysis (Kalnay et al. 1996) winds, geopotential height and NOAA Extended Reconstructed Sea Surface Temperature from 1948-2002 (Smith et al. 1996) are used as major data sources in this study. The CRU (Climatic Research Unit in the University of Norwich, United Kingdom <http://www.cru.uea.ac.uk/>) data based on gauge observations is used for the diagnosis of precipitation. The IOD index as defined by Saji et al. (1999) is used. We further separated the IODs into pure-IOD and ENSO-IOD depending on the coexistence of ENSO events. For the ENSO index, we used Trenberth's (1997) definition. Following the above definitions, 12 positive and 13 negative IOD events are identified (Table 1).

3.The Relation between IOD and

precipitation over Far East Asia

A contrasting anomalous precipitation pattern during the positive and negative phase of IODs is shown in the composite rainfall anomaly maps in Fig. 1. The composite for ENSO without IOD is to separate the sole effect of ENSO from the total effect of ENSO and IOD.

The rainfall anomalies over India show opposite signs for the composites of the IOD with and without ENSO. For El Niño without IOD, the northern part of India is dry and the southern part is wet (Fig. 1c). This is consistent with the findings of Ashok et al. (2004). The rainfall anomalies over Far East Asia also show opposite signs for the composites of the IOD with and without ENSO. The areas over central eastern China, Korea and Japan are dry when the positive IOD occurs without ENSO but wet when El Niño occurs (Fig. 1a, Fig. 1b). The Bonin High over the Yellow Sea, Korea and Japan which was identified as a major factor causing the dry and hot summer over Far East Asia during the positive phase of the IOD (Guan and Yamagata 2003) is evident in the IOD case without ENSO as shown in Fig. 1a.

The impacts of negative IOD and La Niña on the rainfall over Far East Asia appear to be complicated. The Bonin High is active during the negative pure IOD, leading to the dry condition over Korea and the Japan (Fig. 1d). Comparing to the negative pure IOD cases, the anti-cyclonic circulation around Japan during the pure La Niña cases shifts to the north due to the enhancement of the convection over the maritime continent (Fig. 1f). Fig. 1f also shows an anomalous cyclonic circulation stretching from northern Indochina through southern China to the East China Sea when La Niña occurs without IOD. This anomalous cyclone provides a wet condition for Southeast Asia (Ropelewski and Halpert, 1987). When La Niña appears concurrently with negative IOD (Fig. 1e), the anomalous anticyclonic circulation over the South China Sea and the Philippine Sea is substantially intensified, which results in dry

conditions over the areas of Southern China and Taiwan and wet conditions over a wide region from Bangladesh, Assam, the west coast of Myanmar, and the Yangtze River, to Korea and Japan.

The anomalous local Hadley circulation along the longitudes 100°E-120°E in Fig. 2 suggests that both negative IOD and La Niña can enhance the upward motion over Indonesia and the downward motion over the South China Sea. However, for the areas to the north of 20°N, the influence of the IOD is evidently stronger than La Niña. The anomalous subsidence over southern China (25°N-30°N) appears in both pure-IOD (Fig. 2a) and ENSO-IOD (Fig. 2b) plots, but not in the La Niña years without IOD (Fig. 2c). When the negative IOD and La Niña occur together, the anomalous subsidence area extends to the south covering the latitudes of 15°N-25°N. The upward motion over 30°N-35°N is also substantially intensified at the upper-troposphere when the negative IOD and La Niña occur together (Fig. 2b). The surplus rains over Indonesia and central China, Korea and Japan and the deficient rains over the Philippines, southern China and Taiwan resemble the negative phase of Nitta's Pacific-Japan pattern (Nitta 1987), which is explained as a Rossby wave response to the tropical heating over the Philippines by Kurihara and Tsuyuki (1987).

4.Characteristic features of the IODs

Before discussing the time evolution and space characteristics of the IODs, it is important to understand the annual cycle of the Indian Ocean SSTs and equatorial zonal winds. The seasonal evolution of these variables over IOD-W, IOD-E and IOD-U are presented in Fig. 3a. The dominant wind over the central equatorial Indian Ocean is westerly (dashed line) persisting from April to December. The SST over IOD-W is warmest in April and coldest in August due to the strong upwelling induced by the Somali Jet. Therefore, the amplitude of the annual cycle of SST over the IOD-W is much larger

than that over IOD-E. Fig. 3b shows the inter-annual variance of SSTs during the summer monsoon season (JJA). The figure clearly displays that large variances are located near the eastern coast of the Indian Ocean, along Somalia and Saudi-Arabia, and along the western coast of Sumatra. The large variances over IOD-E and IOD-W are due to the IOD.

4.1 Pure-IOD

For the positive pure-IOD, we find that the easterly anomaly first appears over the equatorial Indian Ocean (IOD-U) in March and persists until December (shown as a dashed line in Fig. 4a), while the SST anomaly characterized by negative SSTA over IOD-E and positive SSTA over IOD-W does not appear until May (shown as red and blue lines in Fig. 5a). As the JJA climatology of the zonal wind over IOD-U is westerly (not shown), the easterly anomaly over IOD-U implies weaker westerly winds near the equator. The anomalous easterlies over IOD-U and its associated negative anomalous SST intensify sharply during summer after the Indian summer monsoon matures. The rapid development found in IOD-E does not occur in IOD-W.

The evolution of the negative phase of the pure-IOD is presented in Fig. 5b. Compared with the positive IOD shown in Fig. 5a, the equatorial westerly zonal wind anomaly (dashed line) appears earlier (December of the previous year) and with much smaller amplitude. The development of the SSTA over IOD-E (blue line) starts well before March (Fig. 5b), which is much earlier than the positive IOD case (Fig. 5a).

4.2 ENSO-IOD

For the positive ENSO-IOD, we find that El Niño can enhance the positive SSTA over IOD-W (compare Fig. 5a and 5c). In addition, the anomalous easterly is observed over most of the equatorial Indian Ocean for ENSO associated IOD, but it is much more restricted to the eastern Indian Ocean for positive pure IOD. The

months of initiation, peak and termination of the anomaly over IOD-E are about the same for the positive ENSO- and IOD-oly (Fig. 5a and 5c). Over IOD-W, the time period is shifted forward by several months, due to the effect of ENSO, which normally peaks in winter.

The influence of ENSO on IOD is much greater during the decaying stage of IOD. As the El Niño causes a basin scale warming over the Indian Ocean after its mature phase (Xie et al. 2002; Chowdary and Gnanaseelan 2007), it leads to the warming of IOD-W making the west pole persist longer. The basin scale warming makes the SSTA over IOD-E turn sharply from negative to positive (Fig. 5c) compared to the weak negative SSTA which persisted until the following spring in the pure-IOD case. Thus, characteristic features of the ENSO-IOD during the decaying stage seem to be explained mainly by the superposition of the remote ENSO impact and pure IOD features.

5. Conclusions

The characteristic features of the positive and negative phases of Indian Ocean Dipole events are examined by classifying them into those associated with ENSO (ENSO-IOD) and without (pure-IOD). Our interest is to document the difference in 4 types of IOD, examine their possible impact on Far Eastern Asian monsoon precipitation and to speculate on the differences in the triggering and developing mechanisms of the IODs.

The connection between IOD and the dry/wet precipitation anomaly over Far East Asia is one of the interesting findings in this study. We found that the characteristics of the time evolution and spatial structure of IODs are very different between pure-IOD and ENSO-IOD. The positive and negative pure-IODs also have different evolutions and structures.

Acknowledgements

This study was partially supported by

NSC-96-2745-M-002-010, NSC-96-2625-Z-052-008 and NOAA NA17RJ1231. The views expressed herein are those of the authors and do not necessarily reflect the views of NOAA. We thank Ms. Diane Boomer for the proofreading. Valuable suggestions by three reviewers are highly appreciated.

References

- An, S.-I., and F.-F. Jin, 2004: Nonlinearity and asymmetry of ENSO. *J. Climate*, **17**, 2399-2412.
- Ashok, K., N. H. Saji, and T. Yamagata, 2004: Individual and combined influences of ENSO and Indian Ocean dipole on the Indian summer monsoon. *J. Climate*, **17**, 3141-3155.
- Baquero-Bernal, A., M. Latif, and S. Legutke, 2002: On dipolelike variability of sea surface temperature in the tropical Indian Ocean. *J. Climate*, **15**, 1358-1368.
- Behera, S. K., J.-J. Luo, S. Masson, S. A. Rao, H. Sakuma, and T. Yamagata, 2006: A CGCM study on the interaction between IOD and ENSO. *J. Climate*, **19**, 1688-1705.
- Chowdary, J. S., and C. Gnanaseelan, 2007: Basin-wide warming of the Indian Ocean during El Niño and Indian Ocean dipole years. *Int. J. Climatol.* (in press)
- Dommenget, D., and M. Latif, 2002: A cautionary note on the interpretation of EOFs. *J. Climate*, **15**, 216-225.
- Guan, Z., and Yamagata, T., 2003: The unusual summer of 1994 in East Asia: IOD Teleconnections. *Geophys. Res. Lett.*, **30**, doi:10.1029/2002GL016831..
- Kalnay, E., and coauthors, 1996: The NCEP/NCAR 40-year reanalysis project. *Bull. Amer. Meteor. Soc.*, **77**, 437-472.
- Kug, J.-S., T. Li, I.-S. Kang, J.-J. Luo, S. Masson, and T. Yamagata, 2006: Role of ENSO-Indian coupling on ENSO variability in a coupled GSM. *Geophys. Res. Lett.*, **33**, L09710, doi:10.1029/2005GL024916.
- Kurihara, K., and T. Tsuyuki, 1987: Development of the barotropic high around Japan and its association with Rossby wave-like propagations over the North Pacific:

Analysis of August 1984. *J. Meteor. Soc. Japan*, **65**, 237-246.

Lau, N.-C., and M. J. Nath. 2004: Coupled GCM simulation of atmosphere–ocean variability associated with zonally asymmetric SST changes in the Tropical Indian Ocean. *J. Climate*, **17**, 245–265.

Li, T., B. Wang, C.-P. Chang, and Y. Zang, 2003: A theory for the Indian Ocean dipole-zonal mode. *J. Atmos. Sci.*, **60**, 2119-2135.

Nitta, T., 1987: Convective activities in the Tropical Western Pacific and their impact on the Northern Hemisphere summer circulation. *J. Meteor. Soc. Japan*, **65**, 373-390.

Ropelewski, C. F., and M. S. Halpert 1987: Global and regional scale precipitation patterns associated with the El Niño/Southern Oscillation. *Mon. Wea. Rev.*, **115**, 1606-1626.

Saji, N. H., B. N. Goswami, P. N. Vinayachandran, and T. Yamagata, 1999: A dipole mode in the tropical Indian Ocean. *Nature*, **401**, 360-363.

Saji, N. H., and T. Yamagata, 2003: Structure of SST and surface wind variability during Indian Ocean dipole mode events: COADS observations. *J. Climate*, **16**, 2735-2751.

Smith, T. M., and R. W. Reynolds, R. E. Livezey, and D. C. Stokes, 1996: Reconstruction of historical sea surface temperature using empirical orthogonal functions. *J. Climate*, **9**, 1403-1420.

Trenberth, K. E., 1997: The definition of El Niño. *Bull. Amer. Meteor. Soc.*, **78**, 2771–2777.

Vinayachandran, P. N., N. H. Saji, and T. Yamagata, 1999: Response of the equatorial Indian Ocean to an unusual wind event during 1994. *Geophys. Res. Lett.*, **26**, 1613-1616.

Webster, P. J., A. M. Moore, J. P. Loschnigg, and R. R. Leben, 1999: Coupled ocean-atmosphere dynamics in the Indian Ocean during 1997-1998. *Nature*, **401**, 356-360.

Xie, S. P., H. Annamalai, F. A. Schott, and J. P. McCresry,

2002: Structure and mechanisms of South Indian Ocean climate variability. *J. Climate*, **15**, 864-878.

Yu, J.-Y., and K.-M. Lau, 2004: Contrasting Indian Ocean SST variability with and without ENSO influence: A coupled atmosphere-ocean study. *Meteor. Atmos. Phys.*, **90**, doi:10.1007/s00703-004-0094-7.

Yu, L., and M. M. Rienecker, 1999: Mechanisms for the Indian Ocean warming during the 1997-98 El Niño. *Geophys. Res. Lett.*, **26**, 735-738.

Zhong, A., H. H. Hendon, and O. Alves, 2005: Indian Ocean variability and its association with ENSO in a global coupled model. *J. Climate*, **18**, 3634-3649

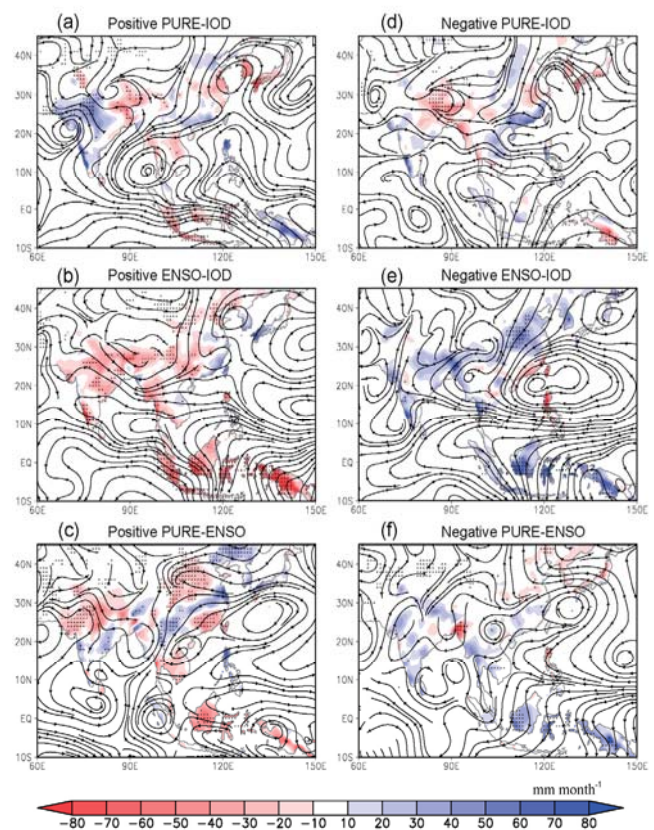


Fig. 1. Composite 850-hPa stream line and precipitation anomaly for JJA during the positive phases of (a) pure-IOD, (b) ENSO-IOD, (c) pure-ENSO, and the negative phases of (d) pure-IOD, (e) ENSO-IOD, and (f) pure-ENSO years. Gray stipples indicate anomalous precipitation is greater than 95% confidence level. The

CRU precipitation is presented. The IOD events are shown in Table 1.

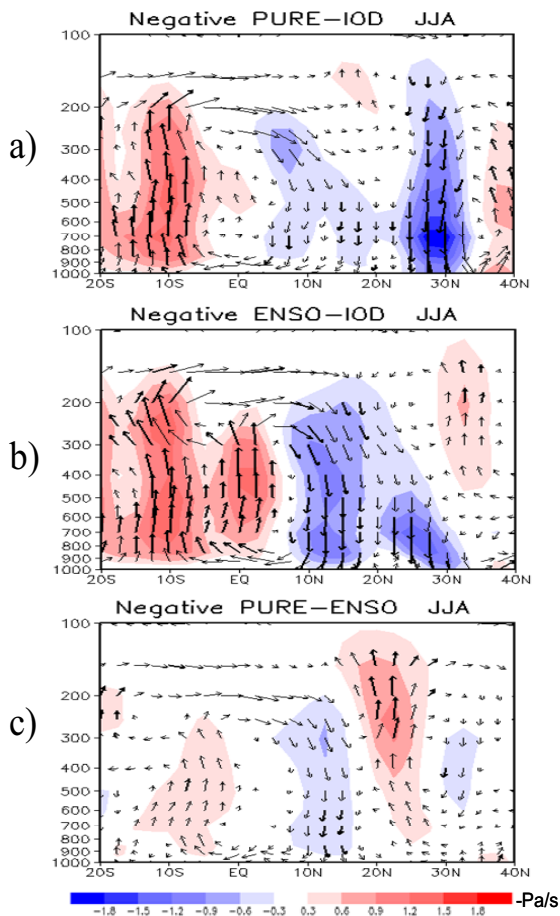


Fig. 2 Composite anomalous JJA local Hadley circulation along the longitudes of 100E-120E represented by the vertical wind velocity (unit: Pa s^{-1}) for the negative phase of (a) pure-IOD, (b) ENSO-IOD, and (c) pure-ENSO. The positive area represents the downward motion and the negative area represents the upward motion. Thick arrows indicate the vertical wind anomaly greater than 95% confidence level.

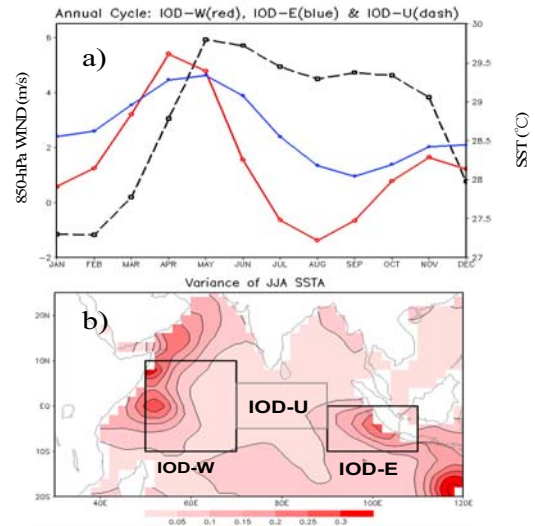


Fig. 3. a) Climatological annual cycle SST over IOD-E (blue line) and IOD-W (red line), and zonal component of wind over IOD-U (dashed line). b) Interannual variance of SST for JJA. The western, central, and eastern boxes represent the areas of IOD-W, IOD-U, and IOD-E respectively.

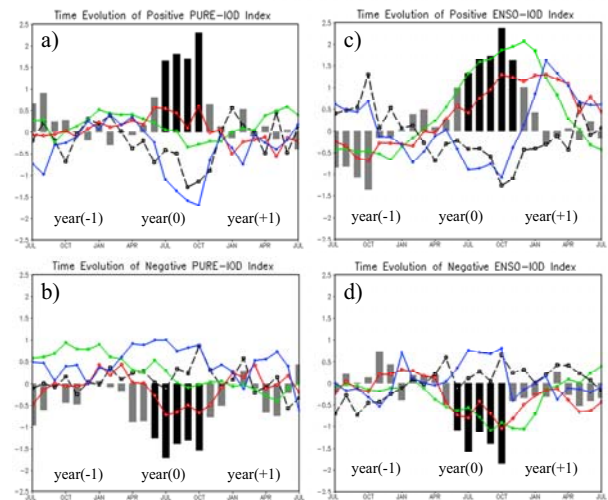


Fig. 4. Time evolution of normalized IOD index (bar), SSTA over IOD-W (red lines), SSTA over IOD-E (blue lines) and zonal wind anomaly over IOD-U (dashed lines). Panel a is for positive pure IOD, b for negative pure IOD, c for positive ENSO-IOD and d for negative ENSO-IOD. The normalized SSTA over Niño3.4 is also shown in green. X-axis is month of the year, (0) being the year when the IOD occurs, (-1) is the previous and (+1) is the following year. Y-axis is normalized variance

Table 1. Years of positive and negative IOD events. The years with asterisks indicate an IOD year with ENSO, and those without indicate a pure-IOD year

Positive IOD	1961,1963*,1966,1967, 1972*,1976*,1977,1982*,1983, 1987*,1994, 1997*
Negative IOD	1954*,1955*,1956*,1958,1959,1960, 1964*,1971*,1989*,1992,1996, 1998*,2001

Table 2. Characteristics of positive and negative phases of pure and ENSO IODs. Season+1 indicates season of the following year, Season-1 indicates season of the previous year. σ is the standard deviation.

		Pure IOD		ENSO-IOD	
Phase		Positive	Negative	Positive	Negative
Evolution		Fast	Slow	Slower than pure IOD positive	Faster than pure IOD negative
IOD-E	anomaly	Cold	Warm	Cold	Warm
	initiation	May	December-1	April-May	April
	peak	October	July	October	October
	termination	December	Jan+1	December	November
	peak amp.	1.8 σ	0.9 σ	1.2 σ	0.7 σ
	maintenance	Ocean adv. Latent heat	Ocean adv. Latent heat	Ocean adv. Latent heat	Ocean adv. Latent heat
IOD-W	anomaly	Warm	Cold	Warm	Cold
	initiation	May	Apr	April-May	April
	peak	Oct	Oct	December	October
	maintenance	Ocean adv.	Ocean adv.	Ocean adv.	Ocean adv. Latent heat
	termination	Jan+1	December	Summer+1	Feb+1
	peak amp.	0.5 σ	0.7 σ	1.3 σ	1.0 σ
IOD-U	anomaly	Easterly	Westerly	Easterly	Westerly
	initiation	April	December -1	March	April
	peak	September	October	October	October
	termination	December	December	May +1	Jan+1
	peak amp.	1.5 σ	0.8 σ	1.4 σ	0.5 σ